Upper Bound Theory for Deformation of Porous Materials

By

Susumu SHIMA*, Tsuyoshi TABATA**, Moriya OYANE*
and Takashi KAWAKAMI***

(Received March 31, 1976)

Abstract

A porous material is idealized in such a way that it possesses an identical yield surface for any volume element throughout the material during a deformation processing. This makes it possible to derive an upper bound theorem on the basis of the plasticity theory for porous metals already proposed by the authors. The theorem is utilized to estimate extrusion pressures and the final density ratios for given initial densities. The estimated values agree well with experimental data.

An alternative way of deriving an upper bound to the load is also presented on a modified yield criterion for porous metals.

1. Introduction

In the previous investigation[1], a plasticity theory for porous metals (already proposed by the authors[2]) has been modified and applied to a few examples of practical forming processes, such as upsetting and closed-die compression of a sintered metal. It has thereby been confirmed that theoretically derived relationships between density and strain, or between working load and density, agree fairly well with the experimental data.

It is a well-known fact that, in general, it is impossible to find out exact solutions for the load to cause plastic deformation in metal forming processes. Therefore, in order to estimate required loads or other relevant values which are necessary for practical processes, attempts have been made to develop various methods to give approximate solutions. Among them, a method for obtaining an upper bound to the load is particularly valuable and widely used.

In case of porous metals, problems involved would be even more complicated due to a significant change in volume during deformation. Thus, it is of great importance

* Department of Mechanical Engineering
** The Osaka Institute of Technology, Omiya, Asahi-ku, Osaka
*** Department of Mechanical Engineering, present address: Sumitomo Heavy Industry

to establish a practical method to obtain approximate solutions.

This paper deals with a proof of an upper bound theorem for deformation of an idealized porous material on the basis of the plasticity theory for porous metals[1),2)]. By the use of the theorem, an approximate solution is presented for the load required in plane-strain extrusion, and then compared with the experimental results for sintered copper.

Further, an alternative way of proving the upper bound theorem is presented, employing the modified yield criterion for porous metals[3)].

2. Upper bound theorem

Since derivation of the upper bound theorem for the conventional plasticity theory is widely known, it will not be explained here.

For convenience, the basic equations for the theory[1),2)] are shown below.

2.1 Basic equations

(i) Yield criterion (or Equation of equivalent stress)*:

$$\sigma_{eq}=\frac{1}{\rho^n}\sqrt{\frac{1}{2}\{(\sigma_x-\sigma_y)^2+(\sigma_y-\sigma_z)^2+(\sigma_z-\sigma_x)^2\}+\left(\frac{\sigma_m}{f}\right)^2+3(\tau_{xy}^2+\tau_{yz}^2+\tau_{zx}^2)} \quad (1)$$

(ii) Stress-strain relations*:

$$\frac{d\varepsilon_x-d\varepsilon_y}{\sigma_x-\sigma_y}=\frac{d\varepsilon_y-d\varepsilon_z}{\sigma_y-\sigma_z}=\frac{d\varepsilon_z-d\varepsilon_x}{\sigma_z-\sigma_x}=\frac{d\gamma_{xy}}{\tau_{xy}}=\frac{d\gamma_{yz}}{\tau_{yz}}=\frac{d\gamma_{zx}}{\tau_{zx}}=\frac{fd\varepsilon_v}{(2/3)(\sigma_m/f)}=\frac{3\,d\varepsilon_{eq}}{2\,\rho^{2n-1}\sigma_{eq}} \quad (2)$$

(iii) Equivalent strain increment*:

$$d\varepsilon_{eq}=\rho^{n-1}\sqrt{\frac{2}{9}\{(d\varepsilon_x-d\varepsilon_y)^2+(d\varepsilon_y-d\varepsilon_z)^2+(d\varepsilon_z-d\varepsilon_x)^2\}+(fd\varepsilon_v)^2+\frac{1}{3}(d\gamma_{xy}^2+d\gamma_{yz}^2+d\gamma_{zx}^2)} \quad (3)$$

where ρ is the density ratio (apparent density of the porous body divided by the pore-free matrix), f is a function of only ρ and n is a positive constant. As in the previous paper[2)], n is chosen to be 2.5 and f is of a form

$$f=\frac{1}{2}\frac{1}{\sqrt{1-\rho}} \quad (4)$$

Plastic work done per unit volume of the porous body is expressed by

* Although the equations have been given in terms of principal stresses and strains in the previous papers[1),2)], it is postulated here that the theory is also valid for a general state of stresses.

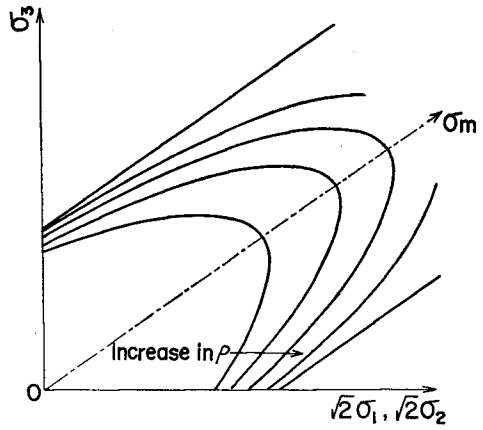

Fig. 1. Yield surfaces with different density ratios

$$dW = \sigma_{ij}\, d\varepsilon_{ij} = \rho\sigma_{eq}\, d\varepsilon_{eq} \tag{5}$$

Fig. 1 shows the yield surfaces in the principal stress space expressed by Eq. (1) with various density ratios when the matrix metal is non-workhardening. In the figure, note that even for the matrix as such, the higher the relative density the larger the yield surface becomes and approaches a cylinder when ρ tends to unity.

2.2 Principle of maximum plastic work

Principle of maximum plastic work for pore-free materials provides

$$\int_V (\sigma'_{ij} - \sigma^{*'}_{ij})\dot{\varepsilon}_{ij} dV \geqq 0$$

for a concave-to-the-origin yield locus, where σ'_{ij} are deviatoric components of stress and $\dot{\varepsilon}_{ij}$ the plastic strain rates related to σ'_{ij} through the associated flow rule. $\sigma^{*'}_{ij}$ are any other deviatoric stress components satisfying the yield criterion. dV refers to a volume element.

A proof of this equation for porous materials is straightforward, replacing σ'_{ij} and $\sigma^{*'}_{ij}$ by the stress components σ_{ij} and σ^{*}_{ij} respectively, provided that the yield surface is concave to the origin (Fig. 1). Thus

$$\int_V (\sigma_{ij} - \sigma^{*}_{ij})\dot{\varepsilon}_{ij} dV \geqq 0 \tag{6}$$

Alternatively, using Eq. (5)

$$\int_V \sigma_{ij}\dot{\varepsilon}_{ij} dV = \int_V \rho\sigma_{eq}\dot{\varepsilon}_{eq} dV \geqq \int_V \sigma^{*}_{ij}\dot{\varepsilon}_{ij} dV \tag{7}$$

Now a porous metal appears to behave like a work-hardening or work-softening material depending on the state of stresses, even if the matrix is perfectly plastic. The former is due to a volume decrease while the latter to a volume increase. Hence,

the yield surface changes during deformation (see Fig. 1). Another complexity is that the density ratio is not uniform throughout the porous body. Therefore, ρ in Eq. (7) is unknown and the integration is impossible.

In order to overcome this problem, the porous body concerned is replaced by an idealized material, such that it possesses an identical yield surface for any volume element throughout the body during a deformation process. The yield surface for this material may in fact be determined by the average density ratio ρ_m, and the yield stress of the rigid-perfectly plastic matrix σ_0, as given by

$$\sigma_0 = \frac{1}{\rho_m^n}\sqrt{\frac{1}{2}\{(\sigma_x-\sigma_y)^2+(\sigma_y-\sigma_z)^2+(\sigma_z-\sigma_x)^2\}+\left(\frac{\sigma_m}{f}\right)^2+3(\tau_{xy}^2+\tau_{yz}^2+\tau_{zx}^2)} \qquad (1)'$$

Then we get

$$\int_V \sigma_{ij}\dot{\varepsilon}_{ij}dV = \rho_m\sigma_0\int_V \dot{\varepsilon}_{eq}dV \geqq \int_V \sigma_{ij}^*\dot{\varepsilon}_{ij}dV \qquad (7)'$$

Note that $\dot{\varepsilon}_{eq}$ also includes ρ_m.

2.3 Upper bound theorem

In the following, a proof is given of an upper bound theorem for porous materials idealized as above.

On a body of volume V and total surface area S, let stresses, strains and other relevant quantities be denoted as follows (Fig. 2):

- v_i : prescribed velocity over the portion of surface S_v
- F_i : surface stresses or surface tractions prescribed over the surface area S_F
- $\dot{\varepsilon}_{ij}$: actual strain rate
- σ_{ij} : actual equilibrium stress field
- v_i^* : any kinematically admissible velocity field, but such that $v_i^*=v_i$ on S_v
- $\dot{\varepsilon}_{ij}^*$: strain rates derived from v_i^*

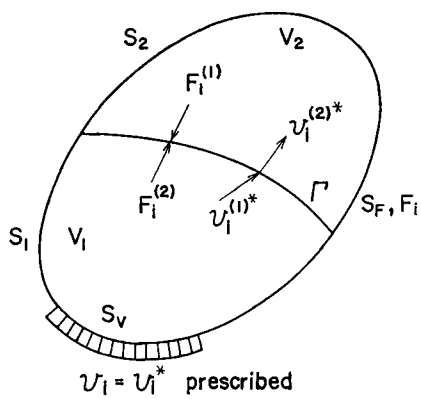

Fig. 2. Definition of terms for use in proof of the theorem

σ^*_{ij} : any stress field which does not violate the yield criterion and derivable by way of the concept of the plastic potential from $\dot{\varepsilon}^*_{ij}$

In fig. 2, Γ is a plane of discontinuity which divides the body of volume V into two regions 1 and 2, the volume and area of which are V_1, V_2 and S_1, S_2 respectively. The principle of virtual work provides the equations,

$$\int_{V_1}\sigma_{ij}\dot{\varepsilon}^*_{ij}dV_1 = \int_{S_1}F_i v^*_i dS_1+\int_\Gamma F^{(1)}_i v^{(1)*}_i d\Gamma$$

for region 1, and

$$\int_{V_2}\sigma_{ij}\dot{\varepsilon}^*_{ij}dV_2 = \int_{S_2}F_i v^*_i dS_2+\int_\Gamma F^{(2)}_i v^{(2)*}_i d\Gamma$$

for region 2, where

$F^{(1)}_i$: a surface stress on Γ exerting from region 2 to 1

$F^{(2)}_i$: a surface stress on Γ exerting from region 1 to 2

$v^{(1)*}_i$: assumed velocity over Γ in region 1

$v^{(2)*}_i$: assumed velocity over Γ in region 2

Equilibrium of stress yields $F^{(1)}_i=-F^{(2)}_i$. Then, adding the above two equations,

$$\int_V\sigma_{ij}\dot{\varepsilon}^*_{ij}dV+\int_\Gamma F^{(1)}_i(v^{(2)*}_i-v^{(1)*}_i)d\Gamma=\int_S F_i v^*_i dS \tag{8}$$

where $V=V_1+V_2$ and $S=S_1+S_2$.

From Eq. (6)

$$\int_V(\sigma^*_{ij}-\sigma_{ij})\dot{\varepsilon}^*_{ij}dV\geqq 0 \tag{9}$$

Applying this to Eq. (8) we get

$$\int_S F_i v^*_i dS \leqq \int_V\sigma^*_{ij}\dot{\varepsilon}^*_{ij}dV+\int_\Gamma F^{(1)}_i(v^{(2)*}_i-v^{(1)*}_i)d\Gamma$$

Now, since $v^*_i=v_i$ on S_v

$$\int_S F_i v^*_i dS = \int_S F_i v_i dS_v+\int_S F_i v^*_i dS_F$$

and consequently

$$\int_{S_v}F_i v_i dS_v \leq \int_V\sigma^*_{ij}\dot{\varepsilon}^*_{ij}dV+\int_\Gamma F^{(1)}_i(v^{(2)*}_i-v^{(1)*}_i)d\Gamma-\int_S F_i v^*_i dS_F \tag{10}$$

In order to determine the 2nd term of the right-hand side of Eq. (10), consider the velocity discontinuity in more detail. For simplicity, only a plane-strain case will be dealt with hereafter. In Fig. 3, Γ is the central line of the shaded area where the velocity changes abruptly. Let t-n coordinate be so chosen that t- and n- axes are respectively tangential and normal to Γ at point 0. Velocity components are denoted by v^*_{t1}, v^*_{n1}, v^*_{t2} and v^*_{n2} as shown in the figure. In contrast to the case of the rigid-perfectly plastic solid, the present body would undergo discontinuity in velocity,

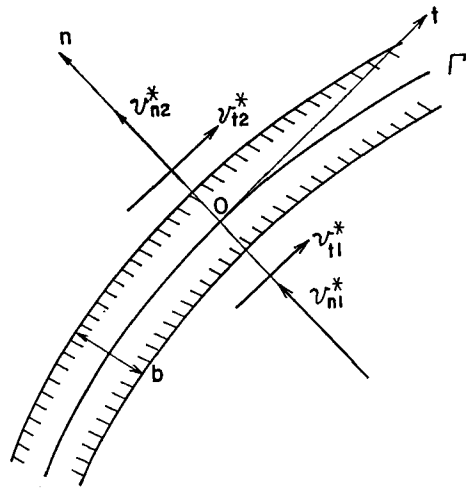

Fig. 3. Definition of terms at a line of velocity discontinuity

not only tangential but also normal to the line of discontinuity as well. In other words, there may be a density difference in the body before and after crossing the line.

Crossing Γ, the material is distorted owing to the velocity discontinuity and thus subjected to strains $\dot{\varepsilon}^*_n$, $\dot{\varepsilon}^*_t$ and $\dot{\gamma}^*_{tn}$ per unit time as given by

$$\left.\begin{aligned} \dot{\varepsilon}^*_n &= \Delta v^*_n/b = (v^*_{n2}-v^*_{n1})/b \\ \dot{\varepsilon}^*_t &= \partial v^*_t/\partial t \end{aligned}\right\} \tag{11}$$

and

$$\dot{\gamma}^*_{tn} = \Delta v^*_t/b+\partial v^*_n/\partial t = (v^*_{t2}-v^*_{t1})/b+\partial v^*_n/\partial t$$

where b is the width of the zone. $\dot{\varepsilon}^*_n$ and $\dot{\varepsilon}^*_t$ are the strain rates the directions of which are respectively normal and tangential to Γ and $\dot{\gamma}^*_{tn}$ the shear strain rate, the other components being zero in plane-strain condition.

Now, the line of velocity discontinuity Γ may be defined as the narrow shaded area whose width b tends to zero (Fig. 3).

The energy dissipated per unit area per unit time along a line element $\delta\Gamma$ is thus described by

$$\delta\dot{W}^* = \lim_{b\to 0} b\sigma_{ij}\dot{\varepsilon}^*_{ij}\delta\Gamma \leqq \lim_{b\to 0} b\sigma^{*\bar{}}_{ij}\dot{\varepsilon}^*_{ij}\delta\Gamma \qquad \text{(See Eq. (9))}$$

Applying Eq. (7)′ to the right-hand side of the above equation, we get

$$\delta\dot{W}^* \leqq \lim_{b\to 0} (b\rho_m\sigma_0\dot{\varepsilon}^*_{eq})\,\delta\Gamma \tag{12}$$

Employing Eq. (3), $\dot{\varepsilon}^*_{eq}$ can be expressed in terms of $\dot{\varepsilon}^*_t$, $\dot{\varepsilon}^*_n$ and $\dot{\gamma}^*_{tn}$ as

$$\dot{\varepsilon}^*_{eq} = \rho_m^{n-1}\sqrt{\frac{2}{9}\{(\dot{\varepsilon}^*_t-\dot{\varepsilon}^*_n)^2+\dot{\varepsilon}^{*2}_n+\dot{\varepsilon}^{*2}_t\}+f^2(\dot{\varepsilon}^*_t+\dot{\varepsilon}^*_n)^2+\frac{1}{3}\dot{\gamma}^{*2}_{tn}}$$

Substituting Eq. (11) into this equation and combining Eq. (12) we get

$$\delta\dot{W}^* \leqq \sigma_0\rho_m^n\sqrt{\left(\frac{4}{9}+f^2\right)\Delta v^{*2}_n+\frac{1}{3}\Delta v^{*2}_t}\ \delta\Gamma$$

and consequently,

$$\int_\Gamma F_i^{(1)}(v_i^{(2)*}-v_i^{(1)*})d\Gamma \leqq \int_\Gamma \sigma_0\rho_m^n\sqrt{\left(\frac{4}{9}+f^2\right)\Delta v^{*2}_n+\frac{1}{3}\Delta v^{*2}_t}\ d\Gamma \tag{13}$$

where f also refers to ρ_m. Substitution of Eq. (13) into (10) yields

$$\int_{S_v} F_i v_i dS_v \leqq \int_V \sigma^*_{ij}\dot{\varepsilon}^*_{ij}dV+\int_\Gamma \sigma_0\rho_m^n\sqrt{\left(\frac{4}{9}+f^2\right)\Delta v^{*2}_n+\frac{1}{3}\Delta v^{*2}_t}\ d\Gamma-\int_{S_F} F_i v^*_i dS_F \tag{14}$$

The right-hand side of Eq. (14) gives an upper bound for the work rate of the unknown surface tractions acting on S_v. A similar equation is obtained when there is more than one line of velocity discontinuity.

If energy is consumed only along the line of discontinuity and further $F_i=0$, Eq. (14) reduces to

$$\int_{S_v} F_i v_i dS_v \leqq \int_\Gamma \sigma_0\rho_m^n\sqrt{\left(\frac{4}{9}+f^2\right)\Delta v^{*2}_n+\frac{1}{3}\Delta v^{*2}_t}\ d\Gamma \tag{14}'$$

When $\rho_m=1$ then $\Delta v^*_n=0$ and Eq. (14)′ reduces to the well-known expression for pore-free solids.

2.3 Plane - strain extrusion

An upper bound to a load required to cause plastic flow may be obtained by minimizing the right-hand side of Eq. (14) under some boundary conditions. However, since the theorem was proved for deformation of the idealized material, the solution obtained should be called an approximate, instead of an upper bound, solution.

In this section, an approximate extrusion pressure and final density ratio will be obtained for a plane - strain case by minimizing the right-hand side of the above theorem.

Half of the extrusion container and the die are shown in Fig. 4(a). Consider the discontinuous velocity pattern shown and the velocity discontinuities occurring along BC and AC. The material to the right of BC moves to the left at unit speed

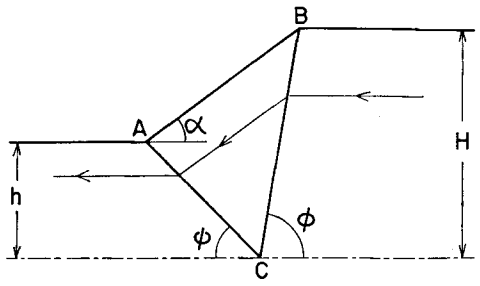

Fig. 4(a). Admissible velocity field

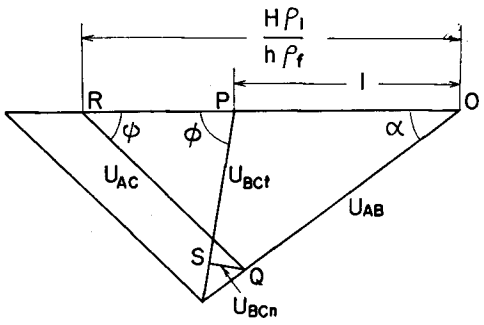

Fig. 4(b). Hodograph

as a rigid block, and successively moves toward the direction of the arrow as indicated. Unless the die face is perfectly smooth, shearing takes place also along the line AB.

Assuming that densification occurs only along BC, then the hodograph which corresponds to the velocity field in Fig. 4(a) is given as shown in Fig. 4(b). In this figure, point R is so chosen that $OR=(H/h)\cdot(\rho_i/\rho_f)$, where ρ_i and ρ_f are the density ratios before and after extrusion respectively. Since, in Fig. 4(a) and (b), BC, AC. and BA are respectively parallel to PS, RQ, and OQ, then if ρ_i and ρ_f are given, point R and hence Q and S are determined. PS, RQ and OQ are the tangential velocity discontinuities occurring along BC, AC and BA respectively, whilst SQ is the normal velocity discontinuity due to the densification along BC. Let $PS=u_{BCt}$, $SQ=u_{BCn}$, $RQ=u_{AC}$ and $OQ=u_{AB}$. From Fig. 4(b) these velocity discontinuities are expressed in terms of ψ, ϕ and α as

$$\left.\begin{aligned} u_{BCt} &= (r-1)\frac{\sin\psi}{\sin(\psi+\phi)}+(r-1)\frac{\sin\phi\cos(\phi+\psi)}{\sin(\psi+\phi)}-r\frac{\sin\alpha\cos(\psi+\phi)}{\sin(\psi+\alpha)} \\ u_{BCn} &= r\frac{\sin\alpha\sin(\psi+\phi)}{\sin(\psi+\alpha)}-(r-1)\sin\phi \\ u_{AC} &= r\frac{\sin\alpha}{\sin(\psi+\alpha)}, \qquad u_{AB}=r\frac{\sin\psi}{\sin(\psi+\alpha)} \end{aligned}\right\} \tag{15}$$

where $r=(H/h)\cdot(\rho_i/\rho_f)$. Lengths of the lines of discontinuities are

$$BC=H/\sin\phi, \quad AC=h/\sin\psi, \quad BA=(H-h)/\sin\alpha \tag{16}$$

In the velocity pattern as shown in Fig. 4(a), energy is consumed only along the lines of discontinuity during extrusion so that the total energy dissipated per unit volume, $\dot{W}$ is given by

Table 1. Δv_n^* and Δv_t^* at each line of velocity discontinuity

	BC	AC	BA
Δv_n^*	u_{BCn}	0	0
Δv_t^*	u_{BCt}	u_{AC}	u_{AB}

$$\dot{W} = \dot{W}_{BC}+\dot{W}_{AC}+\dot{W}_{BA} \tag{17}$$

where W_{BC}, W_{AC} and W_{BA} are energy dissipated along BC, AC and BA respectively. Now there is a relationship between ψ and ϕ as

$$\tan\phi = \frac{1}{(1-h/H)/\tan\alpha-(h/H)/\tan\psi} \tag{18}$$

To obtain an approximate extrusion force, Eq. (14)′ should be used since no back pressure is applied. Using Fig. 4, Δv_n and Δv_t are given for each line of discontinuity as summarized in Table 1. Employing Eq. (18) and Table 1, $\dot{W}_{BC}$, $\dot{W}_{AC}$ and $\dot{W}_{BA}$ are given by

$$\dot{W}^*_{BC} = \sigma_0 H \rho_m^n \sqrt{\left(\frac{4}{9}+f^2\right)(1-\rho_l/\rho_f)^2 + \frac{1}{3}\left[(r-1)\left\{\frac{\cos\alpha}{\sin\alpha}-\frac{\sin(\psi+\alpha)}{R\sin\alpha\cdot\sin\psi}\right\} - r\left\{\frac{\cos(\psi+\alpha)}{\sin(\psi+\alpha)}-\frac{\cos\psi}{R\sin\psi}\right\}\right]^2} \tag{19}$$

where $\rho_m=(\rho_l+\rho_f)/2$ and $f=1/2\sqrt{(1-\rho_m)}$ (see Eq. (4)),

$$\dot{W}^*_{AC} = \rho_f^n \frac{\sigma_0}{\sqrt{3}} Hr \frac{\sin\alpha}{R\sin(\psi+\alpha)\cdot\sin\psi} \tag{20}$$

and

$$\dot{W}^*_{BA} = \rho_f^n \frac{\sigma_0}{\sqrt{3}} mHr \frac{(1-1/R)\sin\psi}{\sin(\psi+\alpha)\cdot\sin\alpha} \tag{21}$$

where $R=H/h$, and $\sigma_0 m/\sqrt{3}$ $(0 \leq m \leq 1)$ is an assumed frictional stress with which the material slides along the die surface.

Using Eq. (14)′ and (17), extrusion pressure p holds an inequality

$$\frac{p}{\sigma_0} \leqq \frac{1}{\sqrt{3}}\left(\rho_m^n \sqrt{3\left(\frac{4}{9}+f^2\right)\left(1-\frac{\rho_l}{\rho_f}\right)^2+\left[(r-1)\left\{\frac{\cos\alpha}{\sin\alpha}-\frac{\sin(\psi+\alpha)}{R\sin\alpha\cdot\sin\psi}\right\}\right.}\right.$$

$$\left.\left.\overline{-r\left\{\frac{\cos(\psi+\alpha)}{\sin(\psi+\alpha)}-\frac{\cos\psi}{R\sin\psi}\right\}\Big]^2}+\rho_f^n\left\{\frac{r\sin\alpha}{R\sin(\psi+\alpha)\cdot\sin\psi}+mr\frac{(1-1/R)\sin\psi}{\sin(\psi+\alpha)\cdot\sin\alpha}\right\}\right) \tag{22}$$

The right-hand side of Eq. (22) is a function of ψ and ρ_f, being noted as $F(\psi, \rho_f)$, with given parameters H, ρ_l, α and m. In the case of a rigid-perfectly plastic solid, the minimum value of $F(\psi, \rho_f)$, where ρ_f is obviously unity, corresponds to the optimum extrusion pressure for the assumed velocity pattern (Fig. 4(a)). For the present case, however, this does not apply. It should be noted that in the former case, the flow stress of the deforming body is a constant, σ_0, whereas in the latter case, it is in fact dependent upon the density ratio, or more precisely, ρ_m. Therefore, if Eq. (22) is rewritten by

$$p/\bar{\sigma}_a \leqq G(\psi, \rho_f) \tag{22}'$$

where $\bar{\sigma}_a$ is the flow stress of the porous material, not of the matrix, the minimum value of $G(\psi, \rho_f)$ would be the optimum solution. $\bar{\sigma}_a$ may be determined as follows. Substituting $\sigma_y=\sigma_z=\tau_{xy}=\tau_{yz}=\tau_{zx}=0$, $\sigma_x=\sigma_1$ into Eq. (1)′, we get

$$\sigma_0 = (1/\rho_m^n)\sqrt{1+1/9f^2}\,|\sigma^1|$$

or

$$|\sigma_1| = (\rho_m^{2.5}/\sqrt{1+1/9f^2})\,\sigma_0 \equiv \bar{\sigma}_a \tag{23}$$

where $\rho_m=(\rho_l+\rho_f)/2$ and $f=1/2\sqrt{(1-\rho_m)}$. Consequently from Eq. (22)′

$$p/\bar{\sigma}_a \leqq \frac{\sigma_0}{\bar{\sigma}_a}\,[F(\psi, \rho_f)] \tag{22}''$$

If σ_0, $\bar{\sigma}_a$ and other parameters are given, $p/\bar{\sigma}_a$ and hence the extrusion pressure p can be estimated with a set of ψ and ρ_f which minimizes $G(\psi, \rho_f)$. The value ρ_f is an approximate density ratio after extrusion.

3. Comparison of the theoretical and experimental results

3.1 Experimental procedures

3.1.1 Powder and preparation of specimens

Electrolytic copper powder was used, details of which are given in Table 2. The powder was compacted in a closed-die to produce parallelepipeds with various densities. They were then sintered at 900°C for 2 hours in a vacuum.

Table 2. Characteristics of copper powder

Apparent density (untapped)	g/cm³	2.0 ~ 2.3
Purity of copper	%	min. 99.6
Oxygen (loss in weight in H_2)	%	max. 0.2

Particle size distribution

mesh	+80	100	145	200	250	350 −
%	max. 3	5~15	30~45	25~35	5~15	max. 10	max. 10

3.1.2 Plane - strain extrusion

The sintered copper was extruded through a die as shown in Fig. 4(a). The extrusion ratio $R(=H/h)$ here was 1.78. Molybdenum-disulphide was used as a lubricant. The extrusion pressure was measured and so was the density of the specimens before and after extrusion.

The density ratio of the specimen after sintering is given in Table 3. Note that prior to the actual onset of extrusion, porous metals are compressed in the container. This matter will be dealt with in a later section.

Table 3. Initial density ratio and effective strain in matrix before extrusion

ρ_i'	0.79	0.855	0.90	0.94
ρ_i	0.915	0.914	0.929	0.951
ε_c	0.19	0.092	0.048	0.018

3.2 Estimation of σ_0 and $\bar{\sigma}_a$

In order to compare the theoretical extrusion pressure with the experimental, σ_0 and therefore, the amount of deformation to which the matrix material is subjected during extrusion must be estimated. As noted above, densification occurs in the container prior to extrusion. Therefore, for estimating the average flow stress of the matrix, the strain in this unsteady state should also be taken into account, which will be determined first. Since this increase in the density cannot be predicted, it was obtained here by measuring the density ratio of the billet (ρ_f), not of the extrudate, after the extrusion test. The compression in the container may be the same as that in a closed-die; and the strain applied to the billet can be estimated (utilizing

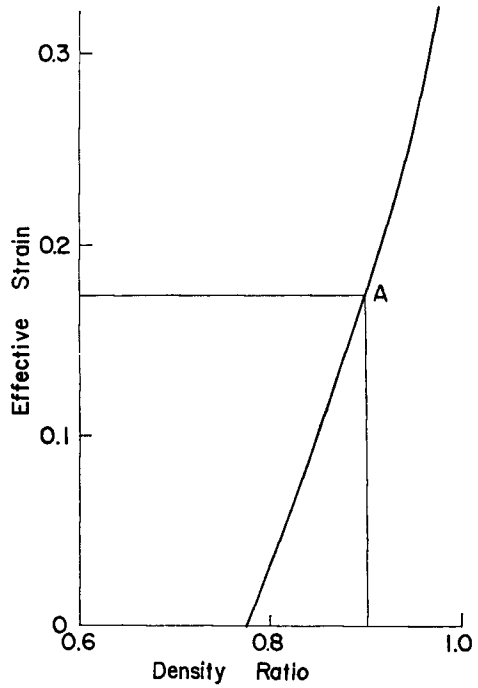

Fig. 5. Relationship between effective strain in matrix metal and density ratio in closed-die compression

Fig. 5[2]) for the four initial densities, as given in Table 3. In the Table, ρ_i' and ρ_l denote the density ratios of the billets before and after extrusion respectively, and ε_c the strain due to the densification.

Secondly, the strain in the steady state extrusion will be estimated. Assumption of ideal deformation during extrusion provides a relationship between the final density ratio and the reduction ratio for a given initial density. This is because the extrusion under this assumption is equivalent to a homogeneous plane - strain compression with a same reduction ratio, as far as the strain to which the matrix is subjected is concerned. Thus, substituting $\sigma_z=\tau_{xy}=\tau_{yz}=\tau_{zx}=0$, $d\varepsilon_x=d\varepsilon_1$, $d\varepsilon_z=d\varepsilon_3$ and $d\varepsilon_y=d\gamma_{xy}=d\gamma_{yz}=d\gamma_{zx}=0$ into Eq. (1)', (2) and (3) and rearranging, the compressive strain increment $d\varepsilon_1$ is expressed in terms of ρ and $d\rho$ as

$$d\varepsilon_1 = -\left\{\frac{2}{3\rho}+\frac{3}{2\rho}\cdot\frac{1}{4(1-\rho)}\right\}d\rho \tag{24}$$

Integration of the equation yields

$$\varepsilon_1 = -\frac{25}{24}\ln\frac{\rho}{\rho_l}+\frac{3}{8}\ln\{(1-\rho)/(1-\rho_l)\} \tag{24}'$$

where ρ_i is an initial density ratio. On the other hand, the strain in plane - strain compression is expressed by

$$\varepsilon_1^* = -\ln\frac{H}{h} = -\ln R \tag{25}$$

where $1-h/H=1-R$ is the reduction ratio. Equating Eq. (24)′ to (25), a relationship is obtained between the initial and final density ratios with a given R. A few of the examples of the relationship are shown in Fig. 6(a). Similarly, $d\varepsilon_3$ is expressed by

$$d\varepsilon_3 = \left(1-\frac{2}{9f^2}\right)(2/3f^2)\frac{d\rho}{\rho}$$

Substituting Eq. (24), $d\varepsilon_y=d\varepsilon_2=0$ and this equation into Eq. (3), we get

$$d\varepsilon_{eq} = \frac{1}{12\sqrt{3}}\frac{\sqrt{(13-4\rho)(25-16\rho)}}{\rho(1-\rho)}|d\rho| \tag{26}$$

Since Eq. (26) is very intricate, the following equation will be utilized instead:

$$d\varepsilon_{eq} = \left(1.132+\frac{0.428}{1-\rho}\right)|d\rho| \tag{26}'$$

which gives a good approximation to Eq. (26). Integration of Eq. (26)′ yields

$$\varepsilon_{eq} = 1.132(\rho-\rho_i)-0.428\ \ln\ \{(1-\rho)/(1-\rho_i)\} \tag{27}$$

Eq. (27) gives the equivalent strain applied to the matrix when a porous material

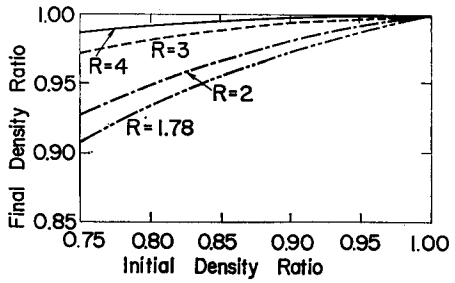

Fig. 6(a). Relationship between initial and final density ratios in plane strain compression

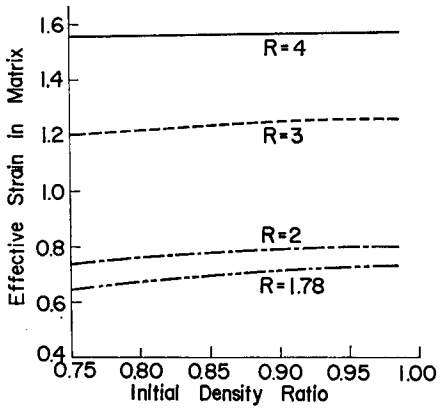

Fig. 6(b). Relationship between effective strain and initial density ratio in plane strain compression

Table 4. σ_0 and $\bar{\sigma}_a$ for each initial density ratio ρ_i

ρ_i	0.915	0.914	0.929	0.951
σ_0 kg/mm²	37.3	35.0	33.35	33.13
$\bar{\sigma}_a$ kg/mm²	31.3	29.2	29.4	30.5

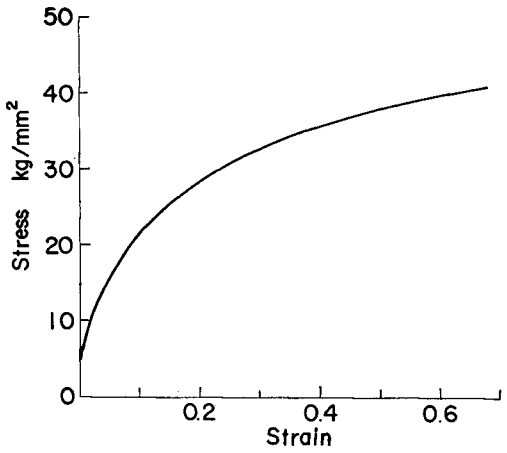

Fig. 7. Stress-strain curve for copper

with an initial density ratio ρ_i is compressed in a plane - strain condition to a final density ratio. Employing this equation coupled with Fig. 6(a), ε_{eq} can be plotted against ρ_i with various R (Fig. 6(b)). Using this figure and extrapolating the stress-strain curve for the matrix[2] (Fig. 7), the average flow stress σ_0 of the matrix during extrusion is given by

$$\sigma_0 = \frac{1}{\varepsilon_f - \varepsilon_c} \int_{\varepsilon_c}^{\varepsilon_f} \sigma_{eq}\, d\varepsilon_{eq} \tag{28}$$

where ε_f is the final strain applied to the matrix. Table 4 gives the values of σ_0 and $\bar{\sigma}_a$ for each initial density ratio.

3.3 Comparison

The estimated values of $p/\bar{\sigma}_a$ [Eq. (22)'] and the corresponding p/σ_0 [Eq. (22)] are obtained for the given shear factors m and plotted against the initial density ratio as in Fig. 8(a). In the figure, the actual extrusion pressure divided by σ_0 and $\bar{\sigma}_a$ is also plotted (4). p/σ_0 increases with an increasing initial density ratio, whereas $p/\bar{\sigma}_a$ is a constant regardless of the initial density. In Fig. 8(b), the final density is plotted against the initial density ratio for $R=1.78$. From the figures, it can be said that, given an appropriate shear factor (here $m=0.3$), the theoretically estimated

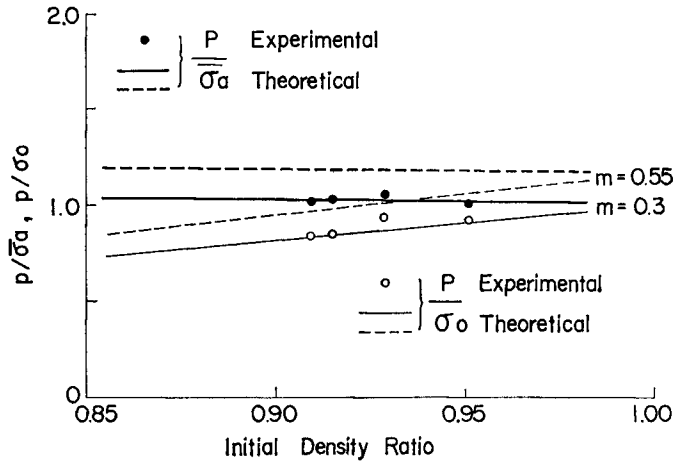

Fig. 8(a). Variation of $p/\bar{\sigma}_a$ and p/σ_0 with initial density ratio of billets in plane-strain extrusion

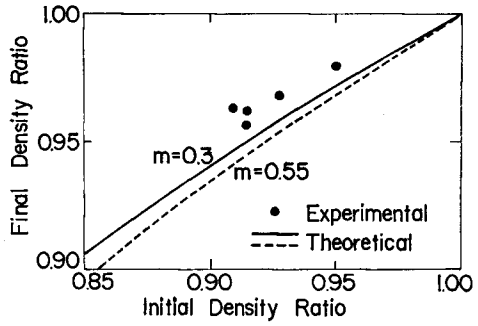

Fig. 8(b). Variation of final density ratio with initial density in plane-strain extrusion

extrusion pressure and the final density ratio agree well with the experimental results for sintered copper.

The curve in Fig. 9 is a calculated curve of non-dimensional extrusion pressure $p/\bar{\sigma}_a$ versus the extrusion ratio R for an initial density ratio of 0.85 and m=0.3. The plots in the figure are the average values after Tabata, et al[4]. There is good agreement between the experimental and the calculated results.

4. Alternative way of proving the upper bound theorem

In the preceding section, an upper bound theorem was proved on the basis of the plasticity theory for porous materials originally proposed by Oyane, et al[1),2)]. In this section, a modified yield criterion will be utilized to prove an upper bound

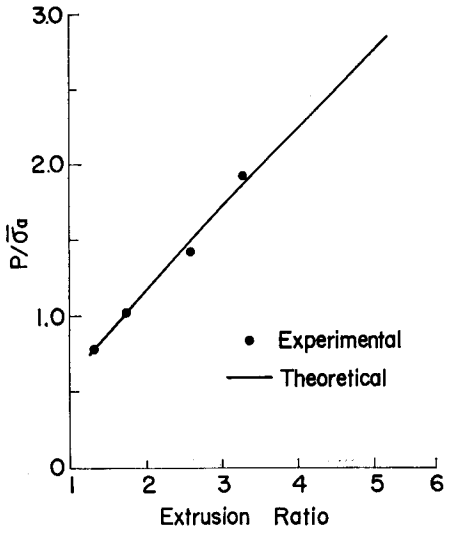

Fig. 9. Variation of $p/\bar{\sigma}_a$ with extrusion ratio in plane strain extrusion (m=0.3)

theorem in a different way.

4.1 Modified yield criterion and associated flow rule

In the original theory, the yield criterion is expressed by Eq. (1), which is an ellipsoid in the principal stress space. Since this yield criterion is rather difficult when applying it to the actual metal forming processes, it is modified in the following way:

$$\sigma_{max}-\sigma_{min}-(\sigma_{max}+\sigma_{min})\sin\theta=\rho^n\sigma_0\cos\theta \qquad \text{for } \sigma_m\leqq 0 \tag{29}$$

$$\sigma_{max}-\sigma_{min}+(\sigma_{max}+\sigma_{min})\sin\theta=\rho^n\sigma_0\cos\theta \qquad \text{for } \sigma_m>0 \tag{30}$$

where σ_{max} and σ_{min} are respectively maximum and minimum principal stresses and θ a function of only ρ. The yield surface expressed by Eqs. (29) and (30) consists of two hexagonal pyramids as shown in Fig. 10. If the height of each pyramid is equalized with, for example, half the length of the major axis of the previous ellipsoid, then θ is expressed in terms of ρ as

$$\tan\theta=1/2f \tag{31}$$

For simplicity, we shall adhere to the plane - strain state in $\sigma_1>\sigma_3>\sigma_2$. If σ_3 is of the same sign as $(\sigma_1+\sigma_2)$, then σ_m can be expressed in terms of $(\sigma_1+\sigma_2)$. Letting $\sigma\equiv(\sigma_1+\sigma_2)/2$ the yield criterion is rewritten as follows:

$$\sigma_1-\sigma_2-2\sigma\sin\theta=\rho^n\sigma_0\cos\theta \qquad \text{for } \sigma\leqq 0 \tag{29}'$$

$$\sigma_1-\sigma_2+2\sigma\sin\theta=\rho^n\sigma_0\cos\theta \qquad \text{for } \sigma>0 \tag{30}'$$

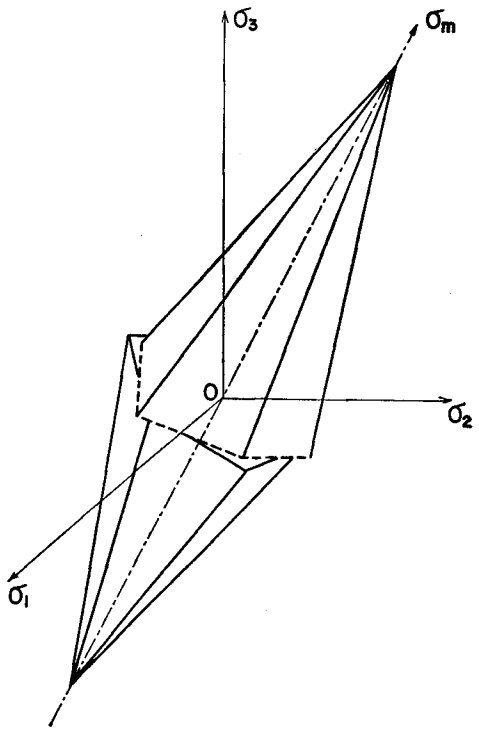

Fig. 10. Modified yield criterion shown in principal stress space

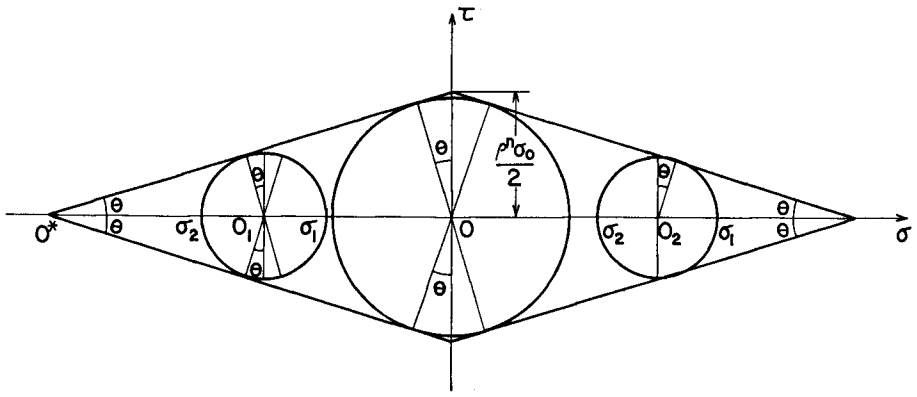

Fig. 11. Modified yield criterion shown in $\sigma-\tau$ plane

σ being called the mean normal stress. Fig. 11 shows the yield criterion in the $\sigma-\tau$ plane. The radius of Mohr's circle 0_1 in the figure is given by

$$a=\frac{\rho^n\sigma_0\cos\theta}{2}+\sigma\sin\theta \tag{32}$$

Because of symmetry, we may deal with the stress state only for $\sigma<0$. The associated flow rule for Eqs. (29)′ and (30)′ provides

$$\dot{\varepsilon}_1 = \dot{\lambda}(1-\sin\theta)$$
$$\dot{\varepsilon}_2 = \dot{\lambda}(-1-\sin\theta) \tag{33}$$

and

$$\dot{\varepsilon}_v=\dot{\varepsilon}_1+\dot{\varepsilon}_2=\dot{\varepsilon}_x+\dot{\varepsilon}_y=-2\dot{\lambda}\sin\theta \tag{34}$$

4.2 Velocity discontinuity

In the section 2.3, the direction of velocity discontinuity vector was taken unknown in the problem concerned, whereas here it will be shown that it is a given parameter so far as the yield criterion (Eqs. (29)′ and (30)′) is employed.

Fig. 12 shows Mohr's circle for the strain rate corresponding to the stress circle shown in Fig. 11. Note that the centre of the strain rate circle, in general, does not coincide with the origin O, since volume constancy does not apply. It has been shown that the directions O_2S_1 and O_2S_2 correspond to those of α- and β- slip lines respectively [3]. When velocity discontinuity exists, the discontinuity line coincides with a slip line. From the figure, the shear strain rate along the discontinuity line is

$$\dot{\gamma}_{s1} = 2\dot{\lambda}\cos\theta \tag{35}$$

Now, let the magnitude of the normal and tangential velocity discontinuity be Δv_x and Δv_y respectively, then we get

$$\dot{\varepsilon}_x = \Delta v_x/b \tag{36-a}$$

and

$$\dot{\gamma}_{xy} = \Delta v_y/b+\partial v_x/\partial y \tag{36-b}$$

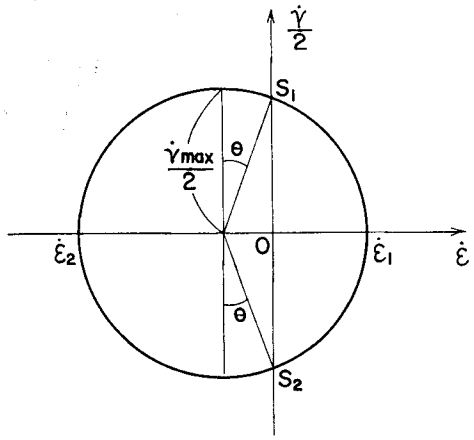

Fig. 12. Strain rate circle corresponding with the stress circle in Fig. 11

In Eq. (36–b), $\partial v_x/\partial y$ is negligible compared with $\Delta v_y/b$, so then $\dot{\gamma}_{xy} \cong \Delta v_y/b$. Further, since the y-direction is the direction of a slip line, then $\dot{\varepsilon}_y=0$. Consequently, we get

$$\dot{\varepsilon}_x = -2\dot{\lambda} \sin\theta \tag{37-a}$$

$$\dot{\gamma}_{xy} = \Delta v_y/b \tag{37-b}$$

Equating Eq. (36–a) with Eq. (37–a), and Eq. (35) with Eq. (37–b), $|\Delta v_x|/|\Delta v_y|$ can be expressed in terms of θ as

$$|\Delta v_x|/|\Delta v_y| = \tan\theta \tag{38}$$

Eq. (38) shows that the velocity discontinuity vector is inclined to the discontinuity line at an angle θ.

4.3 The upper bound theorem

Use the same notations as in section 2.3 except for those of velocity discontinuities Δv_x^* and Δv_y^*, which are respectively normal and tangential to Γ.

Now, Eqs. (9) and (10) obviously hold, which will be written here again:

$$\int_V (\sigma_{ij}^* \dot{\varepsilon}_{ij}^* - \sigma_{ij}\dot{\varepsilon}_{ij}^*) dV \geqq 0 \tag{9}$$

$$\int_{S_v} F_i v_i dS_v = \int_V \sigma_{ij}\dot{\varepsilon}_{ij}^* dV + \int_\Gamma F_i^{(1)}(v_i^{(1)*} - v_i^{(2)*}) d\Gamma - \int_{S_F} F_i v_i^* dS_F \tag{10}$$

Let σ_x and τ_{xy} be the normal and the shear stress components respectively of $F_i^{(1)}$. They are determined from Fig. 10 as

$$|\sigma_x| = (\rho^n \sigma_0/2 - a\cos\theta)\cot\theta/2$$

$$|\tau_{xy}| = a\cos\theta$$

Since $|\Delta v_x^*|/|\Delta v_y^*| = \tan\theta$ (Eq. (38)), the second term of the right-hand side of Eq. (10) can be rewritten by

$$\int_\Gamma F_i^{(1)}(v_i^{(1)*} - v_i^{(2)*}) d\Gamma = \int_\Gamma (|\sigma_x| \cdot |\Delta v_x^*| + |\tau_{xy}| \cdot |\Delta v_y|) d\Gamma$$

$$= \int_\Gamma \frac{\rho^n \sigma_0}{2} \Delta v^* \cos\theta \, d\Gamma \tag{39}$$

where Δv^* is the magnitude of the velocity discontinuity given by

$$\Delta v^* = \sqrt{(\Delta v_x^*)^2 + (\Delta v_y^*)^2}$$

Now, the yield criterion Eq. (29)′ can be expressed in terms of σ_x, with σ_y and τ_{xy} given as

$$g = \sqrt{(\sigma_x - \sigma_y)^2 + 4\tau_{xy}^2} - (\sigma_x + \sigma_y)\sin\theta - \rho^n \sigma_0 \cos\theta$$

Considering g as a plastic potential, the first term of the right-hand side of Eq. (10) holds an inequality

$$\int_V \sigma_{ij}\dot{\varepsilon}^*_{ij}dV \leqq \int_V \sigma^*_{ij}\dot{\varepsilon}^*_{ij}dV = \int_V \frac{\dot{\gamma}_{max}}{2}\rho^n\sigma_0 \cos\theta\, dV \tag{40}$$

Combining Eqs. (10), (39) and (40) we get

$$\int_{S_v} F_i v_i dS_v \leqq \int_V \frac{\dot{\gamma}_{max}}{2}\rho^n\sigma_0 \cos\theta\, dV + \int_\Gamma \frac{\rho^n\sigma_0 \cos\theta}{2}\Delta v^* d\Gamma - \int_S F_i v^*_i dS_F \tag{41}$$

The same equation is obtained for $\sigma > 0$. Eq. (41) gives an upper bound to the work rate of the unknown tractions acting on S_v.

5. Discussion

Although it was first attempted to establish an upper bound theory for porous metals, it appeared to be difficult, if not impossible, due to work-hardening or -softening characteristics resulting from a volume change. Therefore, the porous metal concerned has been idealized such that it possesses an identical yield surface during deformation and throughout the deforming body. This is similar to the case of the conventional upper bound theory for perfectly-plastic solids when applied to work-hardening solids. It is thereby possible to prove an upper bound theorem which gives an approximate extrusion pressure for a sintered metal.

In the velocity field shown in Fig. 4(a), a normal velocity discontinuity may take place also along AC. However, it was not taken into account, since such a discontinuity made the calculation of the energy consumption extremely difficult.

We have derived an upper bound theorem expressed by Eq. (14) or alternatively by Eq. (41). Eq. (41) has an advantage over Eq. (14) when applied to the analysis of actual metal forming processes, e.g., plane strain extrusion [Fig. 4(a), (b)]. The latter involves two variables θ, or the angle which the velocity discontinuity vector PQ makes with PS (Fig. 4(a)) or BC (Fig. 4(b)), and ϕ. In the former, θ is a constant as expressed by, for example, Eq. (31). However, this equation gives an unreasonable overestimation to θ. Therefore, prior to the calculation of Eq. (41) it is necessary to choose an appropriate θ so that it will provide a good estimation to the actual volume change. In employing Eq. (14), on the other hand, the volume change or ρ_f for a given ρ_i in plane strain extrusion is calculated by minimizing the work rate. A similar procedure is applied for Eq. (41), provided that θ is properly determined experimentally [4].

6. Conclusions

On the basis of the plasticity theory for porous metals, an upper bound theorem

was proved for deformation of such an idealized porous body that possessed an identical yield surface for any volume element throughout the body during the deformation process. It was then utilized to estimate an approximate extrusion pressure and also the final density ratio in a plane-strain condition. It was confirmed that the results agree well with experimental data for sintered copper.

This work is a part of a thesis submitted for the degree of Doctor of Engineering in Kyoto University.

References

1) M. Oyane, S. Shima and Y. Kono; Bull. of J. S. M. E., **16,** 1254 (1973).
2) M. Oyane, T. Kawakami and S. Shima; J. Japan Soc. Powder and Powder Met., **20,** 142 (1973).
3) M. Oyane and T. Tabata; J. Japan Soc. Tech. Plasticity, **15,** 43 (1974).
4) T. Tabata and S. Masaki; J. Japan Soc. Tech. Plasticity, **16,** 279 (1975).